Published in final edited form as:
Magn Reson Med. 2012 January ; 67(1): 201–209. doi:10.1002/mrm.22975.

T2-weighted MRI of post-infarct myocardial edema in mice

Ronald J. Beyers[1], **R. Scott Smith**[1,4], **Yaqin Xu**[1], **Bryan A. Piras**[1,4], **Michael Salerno**[2,3], **Stuart S. Berr**[1,2], **Craig H. Meyer**[1,2,4], **Christopher M. Kramer**[2,3,4], **Brent A. French**[1,2,3,4], and **Frederick H. Epstein**[1,2,4,*]

[1]Department of Biomedical Engineering, University of Virginia, Charlottesville, Virginia, USA

[2]Department of Radiology, University of Virginia, Charlottesville, Virginia, USA

[3]Department of Medicine, University of Virginia, Charlottesville, Virginia, USA

[4]Robert M. Berne Cardiovascular Research Center, University of Virginia, Charlottesville, Virginia, USA

Abstract

T2-weighted, cardiac magnetic resonance imaging (T2w CMR) can be used to noninvasively detect and quantify the edematous region that corresponds to the area at risk (AAR) following myocardial infarction (MI). Previously, CMR has been used to examine structure and function in mice, expediting the study of genetic manipulations. To date, CMR has not been applied to imaging of post-MI AAR in mice. We developed a whole-heart, T2w CMR sequence to quantify the AAR in mouse models of ischemia and infarction. The ΔB_0 and ΔB_1 environment around the mouse heart at 7 T were measured, and a T2-preparation sequence suitable for these conditions was developed. Both *in vivo* T2w and late gadolinium enhanced CMR were performed in mice after 20-minute coronary occlusions, resulting in measurements of AAR size of 32.5 ± 3.1 (mean ± SEM) % LV mass, and MI size of 50.1 ± 6.4% AAR size. Excellent interobserver agreement and agreement with histology were also found. This T2w imaging method for mice may allow for future investigations of genetic manipulations and novel therapies affecting the AAR and salvaged myocardium following reperfused MI.

Keywords

T2-weighted; T2w; T2 prep; edema; area at risk; risk area; peri-infarct; mice

Introduction

In occlusive coronary artery disease, the area at risk (AAR) of infarction is defined as the volume of tissue that is perfused, prior to occlusion, by blood flow in coronary arteries distal to an occlusion site. The AAR can be detected after reperfusion using T2-weighted MRI, as the AAR becomes edematous and, consequently, appears hyperintense using this technique (1–3). The area of necrosis, or myocardial infarction (MI), is a subregion of the AAR, and can be delineated using late gadolinium-enhanced (LGE) T1-weighted MRI (4,5). Following reperfusion, the remaining non-necrotic fraction of the AAR, defined as (AAR-MI)/AAR, is called the salvaged area. Maximizing the salvaged area is an aim of both current and new therapies (6–13).

*Correspondence to: Frederick H. Epstein, Ph.D., PO Box 800759, 480 Ray C. Hunt Drive, Charlottesville, VA 22908. FredEpstein@virginia.edu.

Pulse sequences for acquiring T2-weighted cardiac MR (T2w CMR) images have previously been developed for application in humans and large animals. These include turbo spin echo (TSE) with a double inversion-recovery (DIR) preparation (14), TSE steady state free precession (SSFP), and T2-prepared SSFP (15–17). CMR of the AAR would also be useful in imaging studies that employ mice, as mice are widely used to investigate experimental therapies and the roles of individual genes in the setting of MI. However, due to the 10-fold higher heart rate in mice compared to humans, as well as the different off-resonance environment encountered when imaging the mouse heart at field strengths of 4.7 – 14.1 Tesla (T), pulse sequences for T2w CMR that have been previously optimized for imaging humans do not directly apply to mice (18–20).

The overall goal of the present study was to develop T2w CMR methods that can be applied to a mouse model of MI. To accomplish this goal, we (a) measured the variation in B_0 and B_1 in the mouse heart at a field strength of 7 T, (b) designed and developed a pulse sequence for T2w CMR that provides good image quality under the motion, B_1, and off-resonance conditions found in the mouse heart, and (c) evaluated the new sequence for *in vivo* imaging of the AAR and salvaged area.

Materials and Methods

Pulse Sequence

A pulse sequence employing T2 preparation (T2 prep) and a multislice gradient echo readout (GRE), along with combined respiratory gating and ECG triggering, was implemented on a 7 T ClinScan MR system (Bruker, Ettlingen, Germany). Sequence triggers (ECG and respiratory) were produced only during the quiescent phase of expiration to minimize physiologic motion artifacts. The sequence was composed of two independent modules including: 1) a non-selective T2 prep module with flow sensitization (FS) gradients for intraventricular dark blood, and 2) a multislice GRE image acquisition module, as shown in Fig. 1. The T2 prep module was ECG-triggered and applied after an appropriate delay to place the subsequent GRE image acquisition at the next end-diastolic cardiac phase without need for a second ECG trigger. By using a non-selective T2 prep and a multislice readout, whole-heart coverage was achieved with one scan.

The T2 prep module was specifically designed to accommodate the fast heart rate of mice and the ΔB_0 and ΔB_1 environment around the mouse heart at 7 T. We investigated different RF pulse trains for this application with regard to their sensitivity to ΔB_0 and ΔB_1 (21–27). The specific RF refocusing pulses that were compared were singular hard rectangular (rect), composite (90_y:180_x:90_y) hard rect, and fast adiabatic pulse types (25). Our candidate pulse sequences integrated the above refocusing pulse types into Carr-Purcell, Carr-Purcell-Meiboom-Gill, and Malcolm Levitt (CP, CPMG, MLEV) methods. The FS gradients included two mono-polar gradients placed to straddle one of the T2 prep refocusing pulses (28). Although the T2 prep itself is nonselective, these FS gradients were played in the through-plane (slice-select) direction of the GRE image acquisition. This method induces no through-plane net phase accumulation for static tissue while the magnetization from moving blood undergoes dephasing, thereby darkening the intraventricular blood. The FS gradients were placed to play during diastole, when blood inflow is high and when cardiac wall motion is low.

ΔB_0 and ΔB_1 mapping

ΔB_0 and ΔB_1 maps of normal mouse hearts at 7 T were acquired to guide the design requirements of the T2 prep module. To quantify the variation of B_0 and B_1 in a typical mouse heart, we used a two-dimensional (2D) GRE sequence to generate Δf maps and a

modified 2D actual flip angle (AFA) GRE sequence (26,29) to produce ΔB_1 maps. Both sequences were ECG gated to acquire all images at the end-diastolic cardiac phase. GRE images were acquired in short- and long-axis planes. For each plane, a series of images was acquired with echo times (TE) of 1.48 ms to 2.48 ms, at increments of 0.1 ms. Other parameters included TR = 200 ms and slice thickness = 1.0 mm. From this GRE image set, the phase images were then differenced and scaled to produce Δf maps. Likewise, various AFA GRE images in short- and long-axis cardiac planes were acquired with a fixed flip angle of 70 degrees and two different TR times of 5 to 6-fold difference in length, such as, 20 and 120 ms. A detailed discussion of the AFA method may be found in Yarnykh (29). In short, based on analysis of the longitudinal steady-state magnetization, the ratio of the signal strength measured at two repetition times, expressed with their dependence on flip angle, allowed solving for the actual flip angle. The AFA map was then converted to a ΔB_1 map.

Experimental evaluation of T2 prep methods using phantoms

Phantoms were imaged to evaluate the performance of different T2 prep methods under the ΔB_0 and ΔB_1 conditions found *in vivo*. Phantoms were composed of concentrations of agarose gel and copper sulfate that provide T1 and T2 values similar to normal and edematous myocardial tissues at 7 T, with ranges of T1 = 1200 to 1600 ms and T2 = 40 to 100 ms (30). These phantoms were used for sequence testing under both properly-tuned and manually-detuned conditions to investigate sequence sensitivity to inhomogeneous conditions. For these tests, the phantoms were first imaged with the MR scanner precisely tuned, then imaged again after the scanner was incrementally manually detuned (offset) to each of six predetermined levels of Δf up to ±2500 Hz and ΔB_1 up to ±50%.

Image quality of the phantom images was quantified using the structural similarity (SSIM) index method, as described by Wang, *et al* (31). Briefly, the SSIM method compares the structural, intensity, and contrast qualities of modified images to a reference image to produce a [−1, 1] score index, where index = 1 indicates an identical match. The SSIM process first calculates an independent and normalized statistical matrix score for each of the structural, s(x,y), intensity, l(x,y), and contrast, c(x,y) qualities, then combines them into one overall index score. We applied SSIM to quantify changes to image SNR and CNR and to artifacts for each Δf and ΔB_1 image using the respective $\Delta f = 0$ and $\Delta B_1 = 0$ images as the SSIM reference. Before the SSIM calculation, the Δf images were corrected for Δf –induced shifts in the readout direction. This allowed for an objective comparison by evaluating each Δf and ΔB_1 image for degradation in structure, intensity, and contrast.

Animal care and surgical procedure

For animal studies, we used protocols in accordance with the Guide for the Care and Use of Laboratory Animals (NIH publication no. 85-23, Revised 1996). Protocols were approved by the Animal Care and Use Committee at our institution. Ten wild-type male C57Bl/6 mice (11 to 14 wk old; Jackson Laboratories, Bar Harbor, ME) underwent surgically induced MI by a 20-minute occlusion of the left anterior descending (LAD) coronary artery followed by reperfusion. The location along the LAD of the surgical occlusion point was intentionally varied. This was done to ensure the ten mice received differing sizes and locations of MI as well as the corresponding AAR. Briefly, for all surgeries, the mice were anesthetized by intraperitoneal injection of 100 mg/kg pentobarbital sodium and artificially respirated (SAR-830/P ventilator) with an inspired O_2 fraction of 0.80, a frequency of 100 strokes/min, and a tidal volume of 2.0 to 2.5 ml. A parasternal incision was made to open the chest, and the LV was located and exposed. Coronary artery occlusion was achieved by passing a 7-0 silk suture beneath the LAD coronary artery inferior to the left auricle and then tightening it over a length of PE-20 tubing. Successful occlusion was verified by observed ECG measurements with widening of the QRS complex and elevation of the ST segment, along

with visible blanching of the occluded AAR. Reperfusion was achieved by removing the short length of PE-20 tubing. The chest was closed, and 1.0 to 1.5 ml of 5% dextrose was injected intraperitoneally to replace fluids. Throughout the surgery, the mouse body temperature was monitored and maintained at 37.0 ± 0.5 °C.

In vivo CMR preparation and physiological monitoring for mice

Anesthesia was initially induced using 3% isoflurane in the respiratory O_2 delivered via nosecone, and was maintained at a 1% level during imaging. Pediatric ECG leads (Blue Sensor, BRS-50-K/US; Ambu, Linthicum, MD) were attached to the shaved limbs of the mice for cardiac gating. A pneumatic respiration sensor was placed just inferior to the diaphragm for respiratory gating. A length of PE-20 tubing was surgically inserted into the peritoneal cavity for the intraperitoneal (IP) infusion of gadolinium diethylenetriamine pentaacetic acid (Gd-DTPA) contrast agent prior to LGE CMR. ECG, respiration, and body temperature were monitored during imaging using an MRI-compatible system (SA Instruments, Stony Brook, NY). Body temperature was maintained at 37.0 ± 0.5 °C by circulating temperature-controlled warm water under the mice.

CMR imaging

The 7 T scanner (ClinScan, Bruker, Ettlingen, Germany) was equipped with a RF birdcage body coil for mice and gradient system capable of 6.50×10^{-1} T/m maximum strength and 6.667×10^{-3} T·s/m maximum slew rate. Localizer imaging was performed to identify double-oblique long-axis (LA) and short-axis (SA) views of the LV. For supplemental cardiac function data, a four-chamber LA, and a set of six to eight contiguous SA cine images were acquired to cover the entire LV (32). For the T2w sequence, the flow sensitization gradients were set to play in early diastole, when transmitral blood flow is high and dephasing FS gradients are most effective. The multislice GRE acquisition was set to image the same SA slices as the cine sequence. T2w imaging parameters included: CPMG-MLEV weighting with 16 adiabatic refocusing pulses for T2 prep, adiabatic pulse length = 2.4 ms, TR = 3 sec plus the time to the next ECG R-wave (< ≈100 ms), TE = 60 ms, slice thickness = 1.0 mm, BW = 520 Hz/pixel, averages = 2, FOV = 25 × 25 mm, matrix = 128 × 128, and in-plane resolution of 0.20 × 0.20 mm.

In vivo CMR was performed initially on normal mice for sequence development, then later on mice two days after infarct surgery to image AAR and MI. In addition to T2w CMR, LGE CMR was also performed as previously described (33). Briefly, LGE CMR was accomplished by IP injection of Gd-DTPA (0.1 to 0.2 mmol/kg) followed 10 to 15 minutes later by multislice inversion-recovery imaging.

Post-CMR histology

Following completion of all CMR, the mice were euthanized. The hearts were cannulated through the ascending aorta for sequential perfusion with 3 to 4 ml of 1% triphenyltetrazolium chloride (TTC) and 10% phthalocyanine (phthalo) blue (34). To determine the AAR, the LAD was reoccluded with the same suture used for coronary occlusion in preparation for the phthalo blue perfusion. After perfusion, the LV was cut into five to seven transverse slices, mounted on slides and digitally microphotographed. These digital images were processed using ImageJ where the total LV mass, AAR, and MI regions of interest (ROI) were manually traced for each image by an independent analyst kept blind of all CMR results. Specifically, for each histology image, non-phthalo blue indicated the AAR, TTC red/pink indicated viable/non-MI within the AAR (salvaged), and white indicated necrotic MI. From these three ROI, AAR as percent of LV mass, MI as percent of LV mass, MI as percent of AAR, and salvaged area were determined.

CMR image analysis

CMR image analysis was performed using custom programs developed in MATLAB. Each MR image was manually traced to segment the LV myocardium from surrounding tissue. The SNR for an ROI was calculated using the mean magnitude within the ROI divided by the standard deviation (SD) of a background region selected outside the animal. The CNR between two ROI was the difference in SNR between the two ROI. In post-MI mice, a "normal" ROI was selected in the septum, as it was unaffected by occlusion of the LAD coronary artery. For T2w images, myocardial pixels with magnitude greater than the normal ROI mean plus two SD were considered edematous and part of the AAR. For LGE images, myocardial pixels with magnitude greater than the normal ROI mean plus four SD were considered necrotic and part of the MI. These SD threshold values were selected to remain consistent with prior T2w studies (7,35–37), prior LGE studies (3,38,39), and with our own unpublished results from LGE imaging in post-MI mice compared to histological TTC staining. As with the histology data, the MRI data were used to quantify AAR as percent of LV mass, MI as percent of LV mass, MI as percent of AAR, and salvaged area. Tests for statistical significance included the two-tailed Student's *t*-test, where *p*-values less than 0.05 were considered statistically significant. Statistical group results in this study are reported as the mean with standard error of the mean (mean ± SEM). To assess interobserver variability, two independent analysts processed the same T2w CMR images to calculate the AAR. Each analyst performed their own independent segmentation.

Results

ΔB_0 and ΔB_1 mapping

In vivo ΔB_0 and ΔB_1 maps were collected from four normal mice. The ΔB_0 maps measured Δf as ±250 Hz over the majority of the hearts as exemplified in Fig. 2A–2D. However, near the cardiac apex in two of the mice, larger offsets of Δf up to ±1000 Hz were observed. The ΔB_1 maps measured a ±12% variation for typical SA image slices and ±19% variation for typical LA slices, also exemplified in Fig. 2E–2H. Therefore, the *in vivo*, worst-case, ΔB_0 and ΔB_1 mapped levels were $\Delta f = \pm 1000$ Hz and $\Delta B_1 = \pm 19\%$ variation.

Experimental evaluation of T2 prep methods using phantoms

Phantom imaging using the new pulse sequence confirmed the presence of T2 contrast between phantoms representing normal and edematous tissue (40,41). The SNR values for the tissue phantoms were 34.6 and 111.7, providing a CNR of 77.1. Qualitatively, phantoms with similar T1 values but differing T2 values showed excellent contrast while phantoms with differing T1 values and similar T2 values displayed virtually no contrast difference. This supports the presence of strong T2-weighting with minimal T1-weighting.

Figure 3 presents phantom image results comparing the three RF refocusing pulse types under manually detuned Δf and ΔB_1 conditions. These images demonstrate an example where both singular hard rect and composite hard rect pulse types show prominent artifacts for $\Delta f = 1500$ Hz and $\Delta B_1 = 40\%$, whereas adiabatic pulses produce an image without artifacts under the same conditions. The SSIM index graphs, presented in Fig. 4, quantify the performance for each RF pulse type, and illustrate that over a broad range of Δf and ΔB_1, the adiabatic pulses provide the best performance. The SSIM index for both $\Delta f = 0$ Hz and $\Delta B_1 = 0\%$ is 1.0 by definition, since these images were the SSIM reference images. The SSIM index decreases as $|\Delta f|$ and $|\Delta B_1|$ increase for all pulse types. The higher values of SSIM for adiabatic compared to other pulse types reflects their better performance under off-resonance and ΔB_1 conditions. Overall, the adiabatic pulses provided artifact-free performance up to $\Delta f = \pm 1500$ Hz and $\Delta B_1 = \pm 40\%$. This was a three-fold improvement

over singular hard rect and two-fold improvement over composite hard rect pulse performance.

T2-weighted CMR in post-infarct mice

All ten mice underwent successful cine, T2w, and LGE CMR scans, in that order, of the entire LV on day 2 after MI. The T2w CMR acquisition time was approximately 13 minutes, depending on heart and respiratory rates. Figure 5 presents a representative set of T2w CMR LA and SA images from a mouse that had a 20-minute coronary artery occlusion. The images display a hyperintense signal in the AAR, with minimal artifacts. A good spatial correspondence between the AAR and the MI area was achieved, as shown in Fig. 6, with the MI area being a subregion of the AAR. Suppression of intraventricular blood signal achieved using the FS gradients is evident. However, incomplete suppression of low velocity subendocardial blood, especially near the hypokinetic infarcted wall, often occurred (Figs. 5 and 6). For the post-MI group, the SNR for the normal remote myocardium was 45.6 ± 2.6 and the SNR for the hyperintense myocardium was 91.5 ± 5.6, resulting in a CNR of 45.9 ± 3.4.

Comparison of CMR and histology

Following CMR, all ten post-MI mice were euthanized and their hearts were processed for histology. An example comparing LGE imaging, T2w imaging, and histology at matched locations is presented in Fig. 6. The region of hyperintensity on T2w imaging was fully transmural, while the region of gadolinium enhancement was confined to the midwall region. These patterns were common in many data sets, and show that the area of necrosis depicted by LGE is a subset of the AAR as depicted by T2w imaging. For the entire post-MI group, MRI showed that the T2w AAR size was 32.5 ± 3.1 %, and LGE MI size was 17.1 ± 3.1 %. Similarly, histology showed that AAR and MI sizes were 34.1 ± 3.2 and 14.2 ± 2.6 %, respectively. The AAR size measured by T2w CMR was significantly larger than infarct size measured by LGE CMR and histology, both with *p*-values less than 0.002. In addition, measurements of AAR by T2w CMR and histology were not significantly different, and measurements of infarct size by LGE CMR and histology were not significantly different. The scatter plot of Fig. 7A shows good agreement between T2w CMR and histology for measurement of AAR ($R^2 = 0.86$). The corresponding Bland-Altman analysis, presented in Fig. 7B, quantifies a bias of −1.6% for T2w CMR, using histology as a gold standard. The mean MI size as percent AAR size was 50.1 ± 6.4 for mice subjected to a 20-minute coronary occlusion, leading to a salvaged area of 49.9 ± 6.4 percent of the AAR.

Interobserver variability

The scatter plot of Fig. 8A shows good agreement of T2w CMR measurements of AAR size as assessed by two independent and blinded analysts, with excellent linear correlation ($R^2 = 0.91$). The corresponding Bland-Altman analysis, presented in Fig. 8B, indicates a low interobserver bias of −0.15%.

Discussion

We sought to develop methods for performing T2w CMR of the AAR in a mouse model of MI. To overcome challenges associated with the rapid motion of the mouse heart, we investigated a sequence design based on a T2 preparation period followed by a gradient echo readout (21). Because T2 preparation methods can be subject to artifacts related to ΔB_0 and ΔB_1 effects, and because these parameters were previously unknown for our specific application, we measured ΔB_0 and ΔB_1 throughout the mouse heart on a 7 T system. These measurements revealed Δf values as high as ±1000 Hz and ΔB_1 up to ±19 percent. We then compared different RF pulses and pulse trains for these ΔB_0 and ΔB_1 ranges in a series of

phantom experiments. We found that adiabatic pulses combined with a CPMG-MLEV pulse train yielded the best results under these conditions, which agrees with the findings of Nezafat, *et al*, in humans (18). We also employed FS gradient pulses applied during diastolic filling of the LV to dephase the signal from moving blood. The design of these FS gradients was accomplished with care to minimize undesired dephasing of the myocardial tissue signal. The key design features were to place the FS gradients to run at a time of high blood velocity and minimal wall motion, during diastolic filling, and to use a relatively small, per-lobe, gradient area of 4.68×10^{-5} T·s/m and combined first moment of -1.32×10^{-7} T·s^2/m. Under these conditions, experiments in one post-MI mouse showed that SNR in both the infarcted and noninfarcted regions decreased by less than 10% when using the FS gradients compared to using no FS gradients. In general the FS gradients were moderately effective at providing dark blood, with exceptions where blood velocity was reduced, such as near the dysfunctional infarcted LV wall. In such cases, to reduce ambiguity when drawing myocardial borders, our image analysis programs simultaneously displayed the T2w image for segmentation along with cine images at a matched slice location. This simultaneous display provided additional information to the analysts, and helped them draw the borders in a consistent manner. Prior studies (11,12,42) and our preliminary experiments indicated that a T2 prep echo time (TE) of 60 ms gave the best T2w contrast between edematous and normal myocardium. Our multi-slice GRE readout employed a truncated sinc RF pulse. When tested in a normal mouse by comparing a multislice to a single-slice acquisition, slice-to-slice interference led to a 6.2% drop in SNR for multislice imaging. As a whole, the new pulse sequence provided high CNR and minimal artifacts for *in vivo* CMR of the mouse heart at 7 T.

For mice that underwent 20-minute coronary occlusion procedures, T2w CMR measured a mean AAR of 33% of LV mass, which was similar to that measured by histology. Also, LGE T1-weighted CMR found a mean MI size of 17% of LV mass, which was also similar to that measured by histology. The AAR was larger than the MI size for all mice, resulting in a salvaged area that was typically approximately 50% of the AAR. These results parallel the findings of Aletras, *et al*, in canines (11), Garcia-Dorado, *et al*, in swine (12), and O'Regan, *et al*, in humans (9). By varying the coronary artery occlusion site, we were able to evaluate the CMR measurements for AAR's ranging from approximately 20 – 50% of LV mass. Comparisons using linear correlation and Bland-Altman analyses showed good agreement between CMR and histology for both AAR and MI. Interobserver agreement was also very good for assessing the AAR

In future studies these methods may be useful for investigating strategies for increasing the salvaged area after MI. Using a mouse model of MI, genetic manipulations may be readily performed or experimental therapies may be evaluated. In addition, because the AAR, MI, and salvaged area can be quantified noninvasively, these MRI methods should enable studies of AAR, MI, and salvaged area to be combined with longer term post-MI LV remodeling studies. Furthermore, the T2 prep sequence presented here may be easily modified into a T2-mapping sequence by employing multiple TE values. Thus, noninvasive MRI methods may uniquely enable investigators to apply novel therapies and assess both their short-term impact on MI and salvaged area, as well as, their long-term impact on LV remodeling in the same cohort of mice.

Acknowledgments

This work was supported by NIH R01HL092305 to B.A.F. and R01 EB001763 to F.H.E.

References

1. Abdel-Aty H, Cocker M, Meek C, Tyberg JV, Friedrich MG. Edema as a Very Early Marker for Acute Myocardial Ischemia: A Cardiovascular Magnetic Resonance Study. Journal of the American College of Cardiology. 2009; 53(14):1194. [PubMed: 19341860]
2. Edwards N, Routledge H, Steeds R. T2 Weighted Magnetic Resonance Imaging to Assess Myocardial Oedema in Ischemic Heart Disease. Heart. 2009; 10(1136):1–14.
3. Friedrich MG, Abdel-Aty H, Taylor A, Schulz-Menger J, Messroghli D, Dietz R. The Salvaged Area at Risk in Reperfused Acute Myocardial Infarction as Visualized by Cardiovascular Magnetic Resonance. Journal of the American College of Cardiology. 2008; 51(16):1581. [PubMed: 18420102]
4. Kim RJ, Fieno DS, Parrish TB, Harris K, Chen E-L, Simonetti O, Bundy J, Finn JP, Klocke FJ, Judd RM. Relationship of MRI Delayed Contrast Enhancement to Irreversible Injury, Infarct Age, and Contractile Function. Circulation. 1999; 100(19):1992–2002. [PubMed: 10556226]
5. Kim RJ, Wu E, Rafael A, Chen E-L, Parker MA, Simonetti O, Klocke FJ, Bonow RO, Judd RM. The Use of Contrast-Enhanced Magnetic Resonance Imaging to Identify Reversible Myocardial Dysfunction. New England Journal of Medicine. 2000; 343(20):1445–1453. [PubMed: 11078769]
6. Baur L. Magnetic resonance imaging of persistent myocardial obstruction after myocardial infarction. A tool becoming increasingly important in clinical cardiology? The International Journal of Cardiovascular Imaging (formerly Cardiac Imaging). 2009; 25(5):549.
7. Cury RC, Shash K, Nagurney JT, Rosito G, Shapiro MD, Nomura CH, Abbara S, Bamberg F, Ferencik M, Schmidt EJ, Brown DF, Hoffmann U, Brady TJ. Cardiac Magnetic Resonance With T2-Weighted Imaging Improves Detection of Patients With Acute Coronary Syndrome in the Emergency Department. Circulation. 2008; 118(8):837–844. [PubMed: 18678772]
8. Friedrich MG. Myocardial edema -- a new clinical entity? Nat Rev Cardiol. 2010; (7):292–296. [PubMed: 20309007]
9. O'Regan DP, Ahmed R, Neuwirth C, Tan Y, Durighel G, Hajnal JV, Nadra I, Corbett SJ, Cook SA. Cardiac MRI of myocardial salvage at the peri-infarct border zones after primary coronary intervention. Am J Physiol Heart Circ Physiol. 2009; 297(1):H340–H346. [PubMed: 19429834]
10. Stork A, Muellerleile K, Bansmann P, Graessner J, Kaul M, Kemper J, Adam G, Lund G. Value of T2-weighted, first-pass and delayed enhancement, and cine CMR to differentiate between acute and chronic myocardial infarction. European Radiology. 2007; 17(3):610. [PubMed: 17149626]
11. Aletras AH, Tilak GS, Natanzon A, Hsu L-Y, Gonzalez FM, Hoyt RF Jr, Arai AE. Retrospective Determination of the Area at Risk for Reperfused Acute Myocardial Infarction With T2-Weighted Cardiac Magnetic Resonance Imaging: Histopathological and Displacement Encoding With Stimulated Echoes (DENSE) Functional Validations. Circulation. 2006; 113(15):1865–1870. [PubMed: 16606793]
12. Garcia-Dorado D, Oliveras J, Gili J, Sanz E, Pérez-Villa F, Barrabés J, Carreras MJ, Solares J, Soler-Soler J. Analysis of myocardial oedema by magnetic resonance imaging early after coronary artery occlusion with or without reperfusion. Cardiovascular Research. 1993; 27(8):1462–1469. [PubMed: 8297415]
13. Garcia-Dorado D, Ruiz-Meana M, Piper HM. Lethal reperfusion injury in acute myocardial infarction: facts and unresolved issues. Cardiovascular Research. 2009; 83(2):165–168. [PubMed: 19502282]
14. Simonetti OP, Finn JP, White RD, Laub G, Henry DA. "Black blood" T2-weighted inversion-recovery MR imaging of the heart. Radiology. 1996; 199(1):49–57. [PubMed: 8633172]
15. Aletras AH, Kellman P, Derbyshire JA, Arai AE. ACUT2E TSE-SSFP: A hybrid method for T2-weighted imaging of edema in the heart. Magnetic Resonance in Medicine. 2008; 59(2):229–235. [PubMed: 18228588]
16. Kellman P, Aletras AH, Mancini C, McVeigh ER, Arai AE. T2-prepared SSFP improves diagnostic confidence in edema imaging in acute myocardial infarction compared to turbo spin echo. Magnetic Resonance in Medicine. 2007; 57(5):891–897. [PubMed: 17457880]

17. Shea SM, Fieno DS, Schirf BE, Bi X, Huang J, Omary RA, Li D. T2-prepared Steady-State Free Precession Blood Oxygen Level-Dependent MR Imaging of Myocardial Perfusion in a Dog Stenosis Model. Radiology. 2005; 236(2):503–509. [PubMed: 16040907]
18. Nezafat R, Stuber M, Ouwerkerk R, Gharib A, Desai M, Pettigrew R. B1-insensitive T2 preparation for improved coronary magnetic resonance angiography at 3 T. Magnetic Resonance in Medicine. 2006; 55(4):858–864. [PubMed: 16538606]
19. Norris DG. Adiabatic radiofrequency pulse forms in biomedical nuclear magnetic resonance. Concepts in Magnetic Resonance. 2002; 14(2):89–101.
20. Zweckstetter M, Holak TA. An Adiabatic Multiple Spin-Echo Pulse Sequence: Removal of Systematic Errors Due to Pulse Imperfections and Off-Resonance Effects. Journal of Magnetic Resonance. 1998; 133(1):134. [PubMed: 9654478]
21. Brittain J, Hu B, Wright G, Meyer C, Macovski A, Nishimura D. Coronary Angiography with Magnetization-Prepared T2 Contrast. Magnetic Resonance in Medicine. 1995; 33(5):689–696. [PubMed: 7596274]
22. De Graaf R A, Nicolay K. Adiabatic rf pulses: Applications to in vivo NMR. Concepts in Magnetic Resonance. 1997; 9(4):247–268.
23. Hürlimann MD. Carr-Purcell Sequences with Composite Pulses. Journal of Magnetic Resonance. 2001; 152(1):109. [PubMed: 11531370]
24. Sung KaN KS. SAR-Constrained Saturation Pulse Designs Based on B0 and B1 Maps. Proceedings International Society of Magnetic Resonanance in Medicine. 2008; 16:228.
25. Tannús A, Garwood M. Adiabatic pulses. NMR in Biomedicine. 1997; 10(8):423–434. [PubMed: 9542739]
26. Treier R, Steingoetter A, Fried M, Schwizer W, Boesiger P. Optimized and combined T1 and B1 mapping technique for fast and accurate T1 quantification in contrast-enhanced abdominal MRI. Magnetic Resonance in Medicine. 2007; 57(3):568–576. [PubMed: 17326175]
27. Ugurbil K, Garwood M, Rath AR, Bendall MR. Amplitude-Modulated And Frequency Phase-Modulated Refocusing Pulses That Induce Plane Rotations Even In The Presence Of Inhomogeneous B1 Fields. Journal Of Magnetic Resonance. 1988; 78(3):472–497.
28. Bernstein, M.; King, K.; Zhou, X. Handbook of MRI Pulse Sequences. Burlington: Elsevier Academic Press; 2004. Flow-Encoding Gradients; p. 281-286.
29. Yarnykh VL. Actual flip-angle imaging in the pulsed steady state: A method for rapid three-dimensional mapping of the transmitted radiofrequency field. Magnetic Resonance in Medicine. 2007; 57(1):192–200. [PubMed: 17191242]
30. Kato H, Kuroda M, Yoshimura K, Yoshida A, Hanamoto K, Kawasaki S, Shibuya K, Kanazawa S. Composition of MRI phantom equivalent to human tissues. Medical Physics. 2005; 32(10):3199. [PubMed: 16279073]
31. Wang Z, Bovik AC, Sheikh HR EPS. Image quality assessment: From error visibility to structural similarity. IEEE Transactions on Image Processing. 2004; 13(4):600–612. [PubMed: 15376593]
32. Berr SS, Rene RJ, French BA, Yang Z, Gilson W, Kramer CM, Epstein FH. Black blood gradient echo cine magnetic resonance imaging of the mouse heart. Magnetic resonance in medicine. 2005; 53(5):1074. [PubMed: 15844138]
33. Helm PA, Caravan P, French BA, Jacques V, Shen L, Xu Y, Beyers RJ, Roy RJ, Kramer CM, Epstein FH. Postinfarction Myocardial Scarring in Mice: Molecular MR Imaging with Use of a Collagen-targeting Contrast Agent1. Radiology. 2008; 247(3):788–796. [PubMed: 18403626]
34. Xu Y, Huo Y, Toufektsian M-C, Ramos SI, Ma Y, Tejani AD, French BA, Yang Z. Activated platelets contribute importantly to myocardial reperfusion injury. Am J Physiol Heart Circ Physiol. 2006; 290(2):H692–H699. [PubMed: 16199480]
35. Abdel-Aty H, Zagrosek A, Schulz-Menger J, Taylor AJ, Messroghli D, Kumar A, Gross M, Dietz R, Friedrich MG. Delayed Enhancement and T2-Weighted Cardiovascular Magnetic Resonance Imaging Differentiate Acute From Chronic Myocardial Infarction. Circulation. 2004; 109(20): 2411–2416. [PubMed: 15123531]
36. Phrommintikul A, Abdel-Aty H, Schulz-Menger J, Friedrich MG, Taylor AJ. Acute oedema in the evaluation of microvascular reperfusion and myocardial salvage in reperfused myocardial

infarction with cardiac magnetic resonance imaging. European Journal of Radiology. 2009; 74(3):e12. [PubMed: 19375879]

37. Wright J, Adriaenssens T, Dymarkowski S, Desmet W, Bogaert J. Quantification of Myocardial Area at Risk With T2-Weighted CMR: Comparison With Contrast-Enhanced CMR and Coronary Angiography. JACC: Cardiovascular Imaging. 2009; 2(7):825. [PubMed: 19608131]
38. Amado LC, Gerber BL, Gupta SN, Rettmann DW, Szarf G, Schock R, Nasir K, Kraitchman DL, Lima JAC. Accurate and objective infarct sizing by contrast-enhanced magnetic resonance imaging in a canine myocardial infarction model. Journal of the American College of Cardiology. 2004; 44(12):2383. [PubMed: 15607402]
39. Kwong RY, Schussheim AE, Rekhraj S, Aletras AH, Geller N, Davis J, Christian TF, Balaban RS, Arai AE. Detecting Acute Coronary Syndrome in the Emergency Department With Cardiac Magnetic Resonance Imaging. Circulation. 2003; 107(4):531–537. [PubMed: 12566362]
40. Mitchell MD, Kundel HL, Axel L, Joseph PM. Agarose as a tissue equivalent phantom material for NMR imaging. Magnetic Resonance Imaging. 1986; 4(3):263. [PubMed: 3669940]
41. Yang QX, Wang J, Collins CM, Smith MB, Zhang X, Ugurbil K, Chen W. Phantom design method for high-field MRI human systems. Magnetic Resonance in Medicine. 2004; 52(2):1016–1020. [PubMed: 15508165]
42. Wisenberg G, Prato FS, Carroll SE, Turner KL, Marshall T. Serial nuclear magnetic resonance imaging of acute myocardial infarction with and without reperfusion. American Heart Journal. 1988; 115(3):510. [PubMed: 3344656]

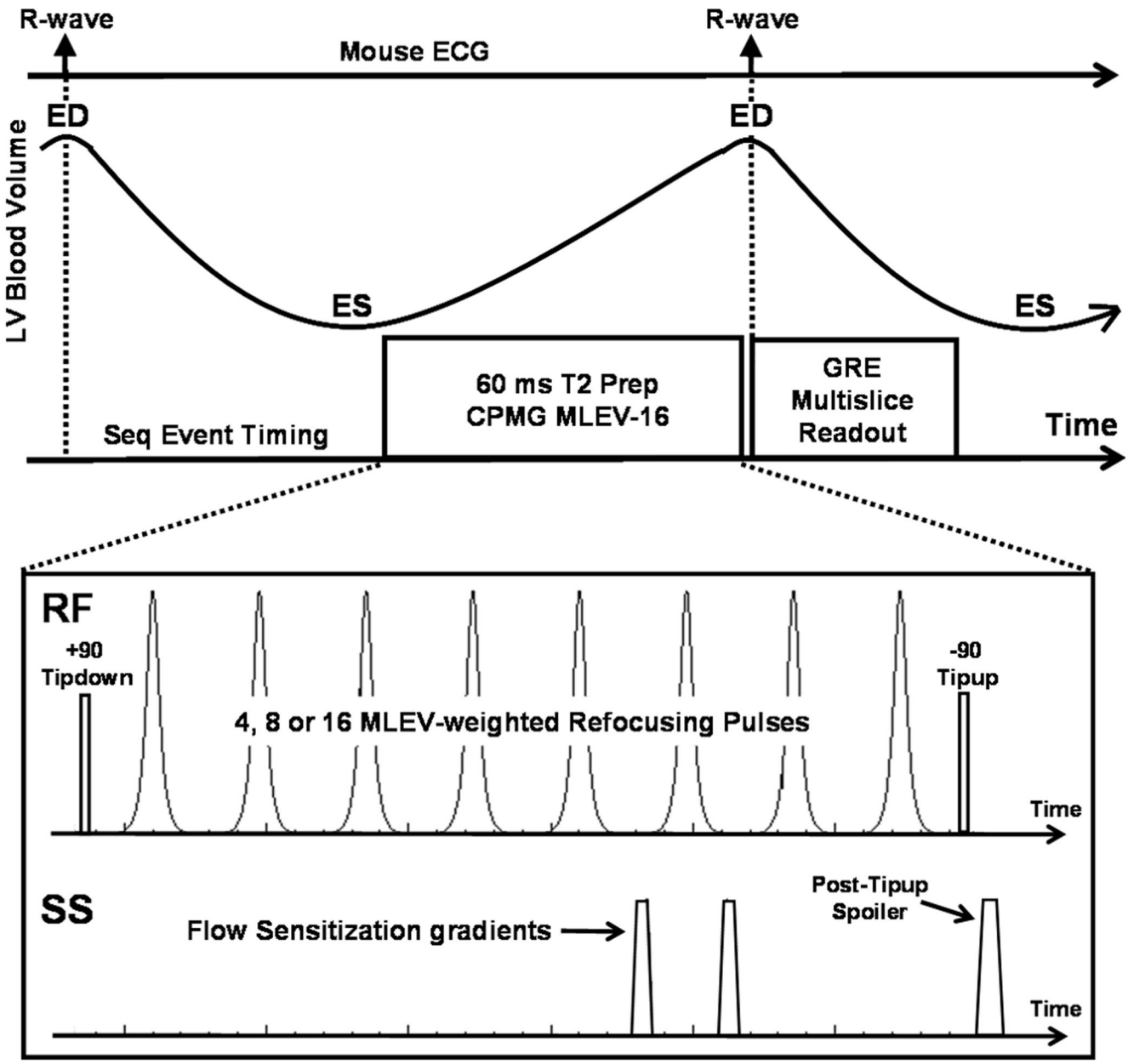

Figure 1.

T2-weighted CMR pulse sequence design. For T2 preparation, a non-selective Carr-Purcell-Meiboom-Gill, Malcolm Levitt (CPMG-MLEV) pulse train is used comprising adiabatic RF pulses and flow sensitization (FS) gradients. For data sampling, a multislice gradient echo readout is used. ED: end-diastole, ES: end-systole.

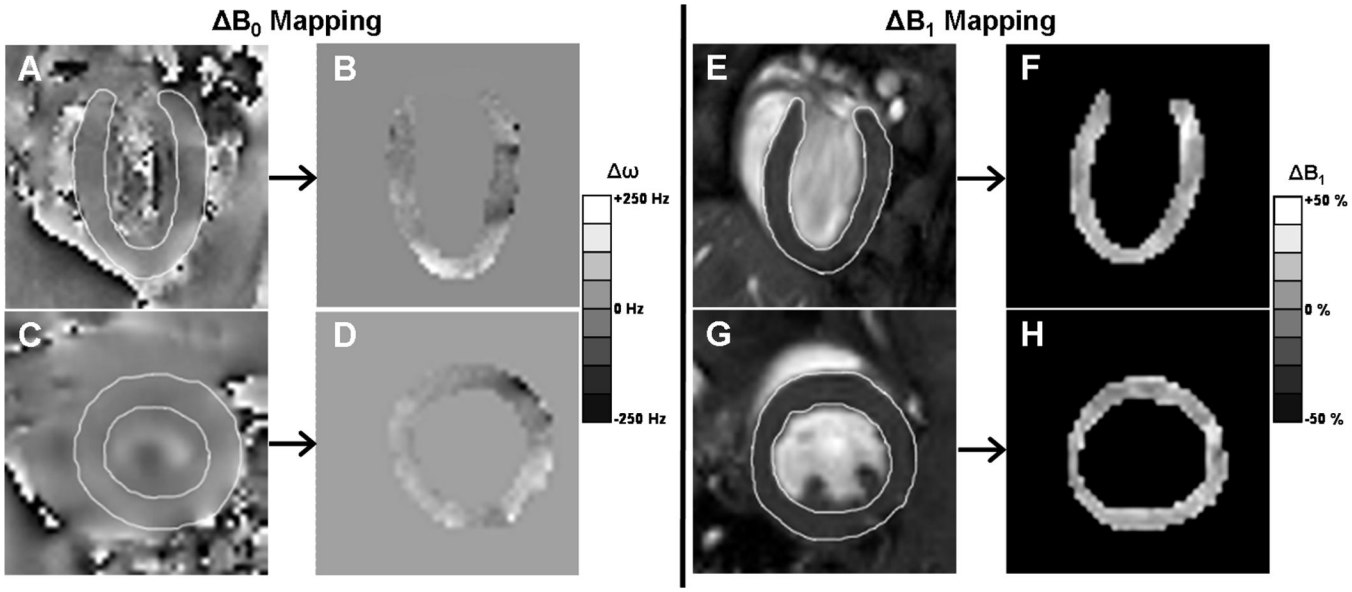

Figure 2.

Representative long- and short-axis (LA, SA) cardiac ΔB_0 (as Δf) and ΔB_1 maps from mice imaged at 7 Tesla. Panels A and C display phase-reconstructed gradient echo ΔB_0 maps with corresponding panels B and D displaying the segmented and scaled Δf maps for the myocardium. Panels E and G display actual flip angle (AFA) B_1 magnitude-ratio maps with corresponding panels F and H displaying the segmented and scaled ΔB_1 maps for the myocardium. Overall, Δf was generally in the range of ±250 Hz and ΔB_1 was in the range of ±19% throughout the LV. Occasionally measurements showed Δf up to ±1000 Hz at air-tissue interfaces.

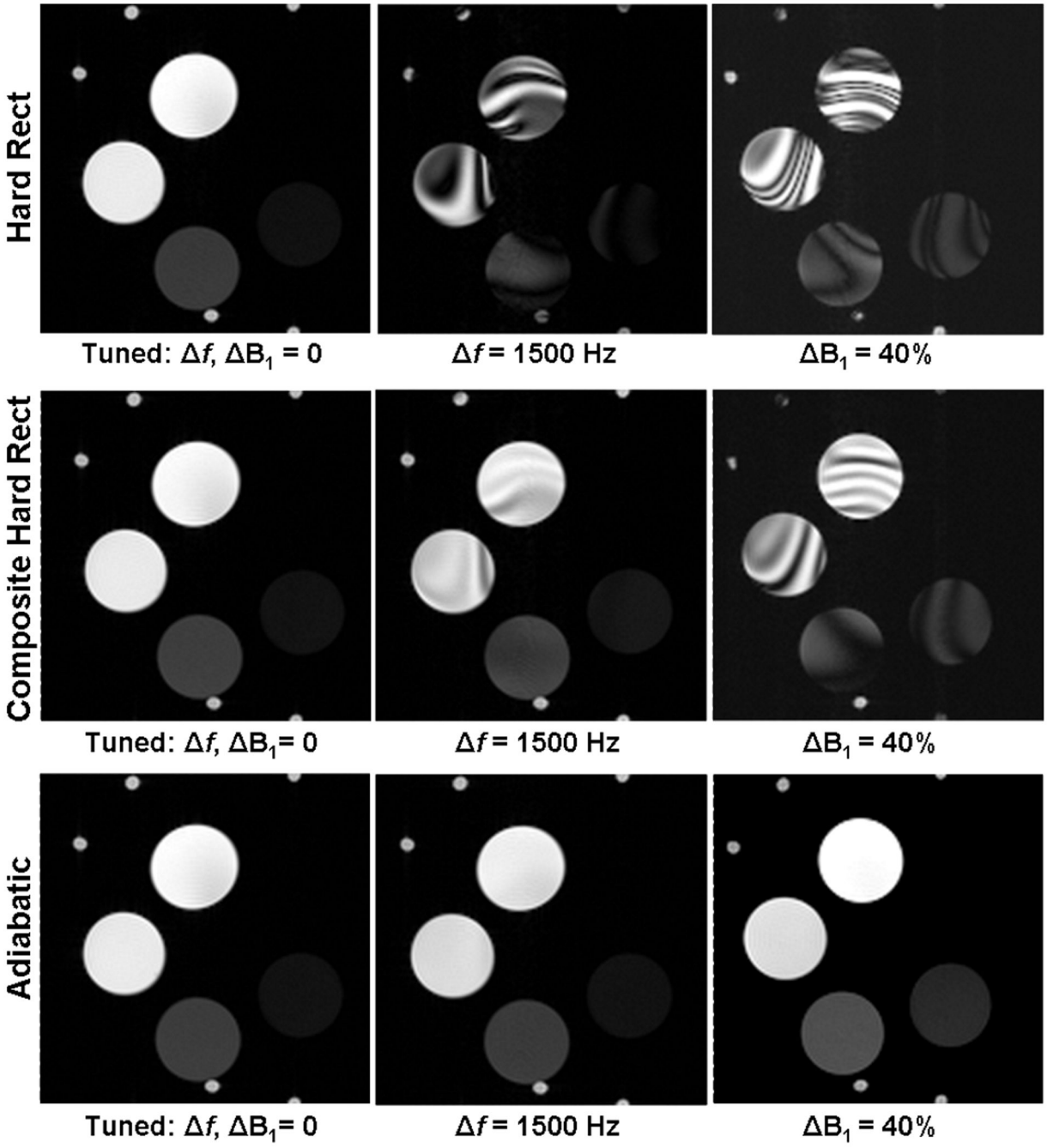

Figure 3.

Representative T2w CMR phantom images comparing performance of RF refocusing pulse types including singular hard rect (top row), composite hard rect (middle row), and adiabatic (bottom row). Optimally tuned images (left column) are artifact free for all pulse types, while at manually detuned Δf = 1500 Hz (center column) and ΔB_1 = 40% (right column), the images remain artifact free for only the adiabatic pulse type while both singular hard rect and composite hard rect types produce prominent artifacts.

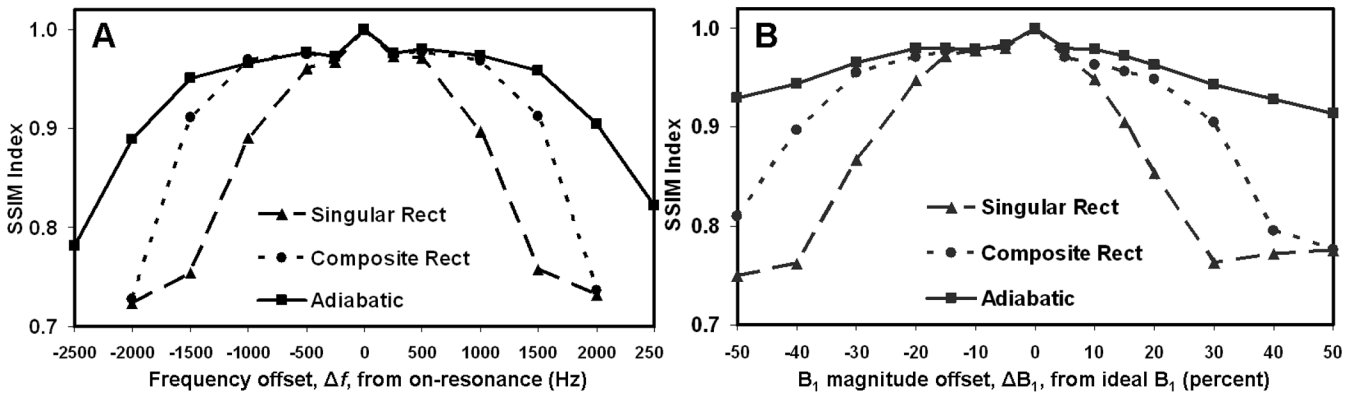

Figure 4.

Structural similarity (SSIM) index was used to quantify the quality of T2w CMR in phantoms at a range of off-resonance and ΔB_1 conditions for different RF refocusing pulse types. On-resonance ($\Delta f = 0$) and off-resonance (Δf up to ±2500 Hz) SSIM results (A). Ideal ($\Delta B_1 = 0$) and ΔB_1 up to ±50% SSIM results (B). For both graphs, ideally tuned conditions corresponded to SSIM index = 1. Both graphs demonstrate that the adiabatic pulse type is least sensitive to changes in Δf and ΔB_1.

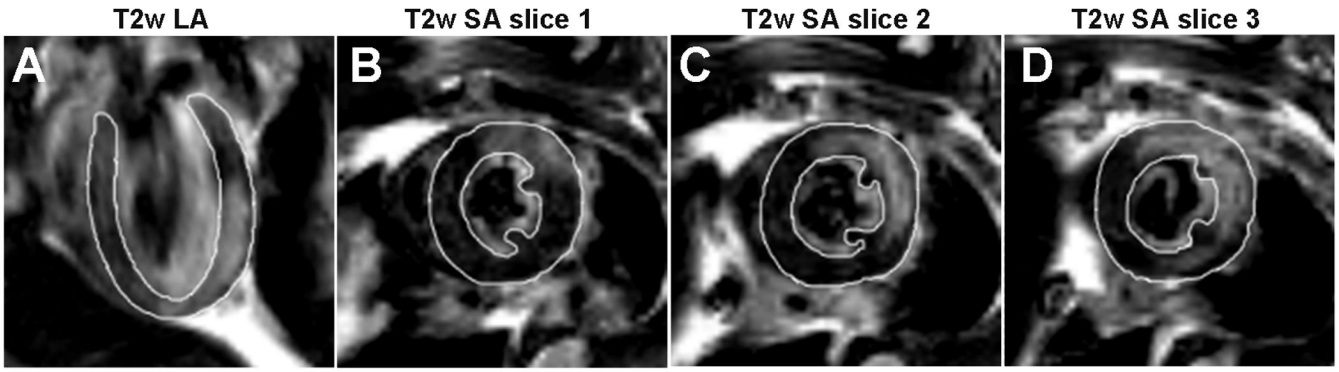

Figure 5.

Representative T2-weighted images of the mouse heart acquired 2 days after inducing an experimental myocardial infarction. One long-axis view (A) and three consecutive short-axis views (B – D) are shown. Regions of myocardial hyperintensity appear in the anterolateral wall, commensurate with edema in the area at risk (AAR) corresponding to a left anterior descending (LAD) arterial occlusion. The segmentation lines delineating the myocardium were hand-drawn. The signal from intraventricular blood was partially suppressed using flow sensitization gradients.

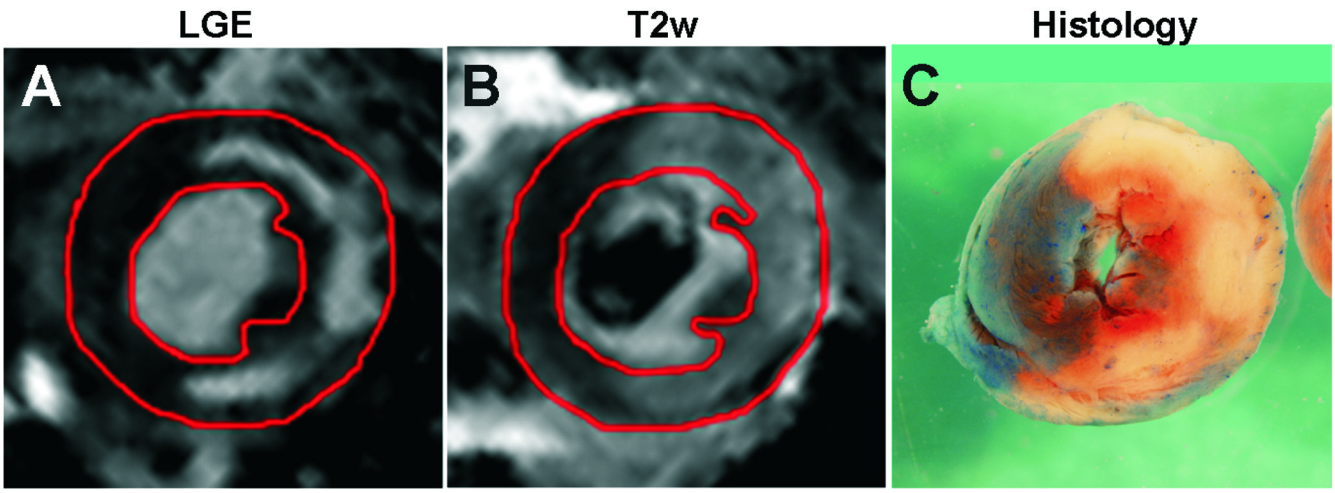

Figure 6.
In matched slices of a mouse heart acquired 2 days after a 20-minute coronary artery occlusion, the area of infarction as assessed by hyperintensity on late gadolinium-enhanced (LGE) T1-weighted CMR (A) is a subregion of the area at risk (AAR) as assessed by hyperintensity on T2-weighted CMR (B). Histology of the same slice is shown in (C), where non-blue indicates AAR, white indicates necrotic infarction, red/pink indicates the salvaged area.

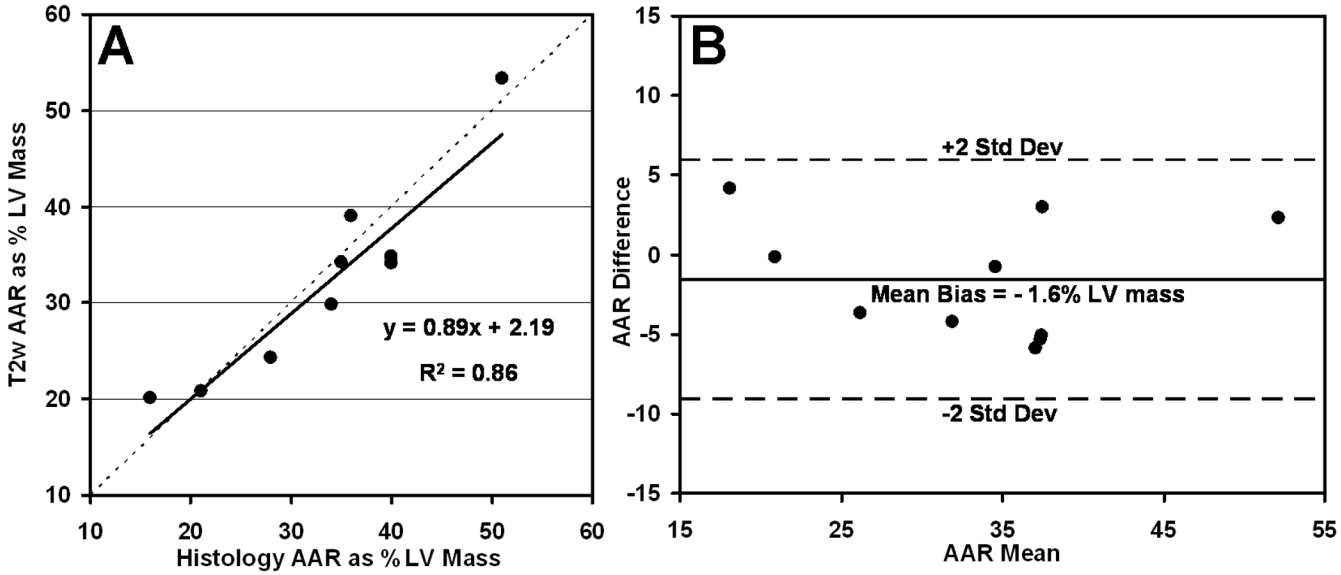

Figure 7.

Comparison of area at risk (AAR) size measured by T2-weighted CMR and histology. Scatter plot of AAR size as percent LV mass shows good linear correlation ($R^2 = 0.86$) between T2w CMR and histology (A). Bland-Altman analysis indicates a bias of −1.6% for T2w CMR compared to histology (B).

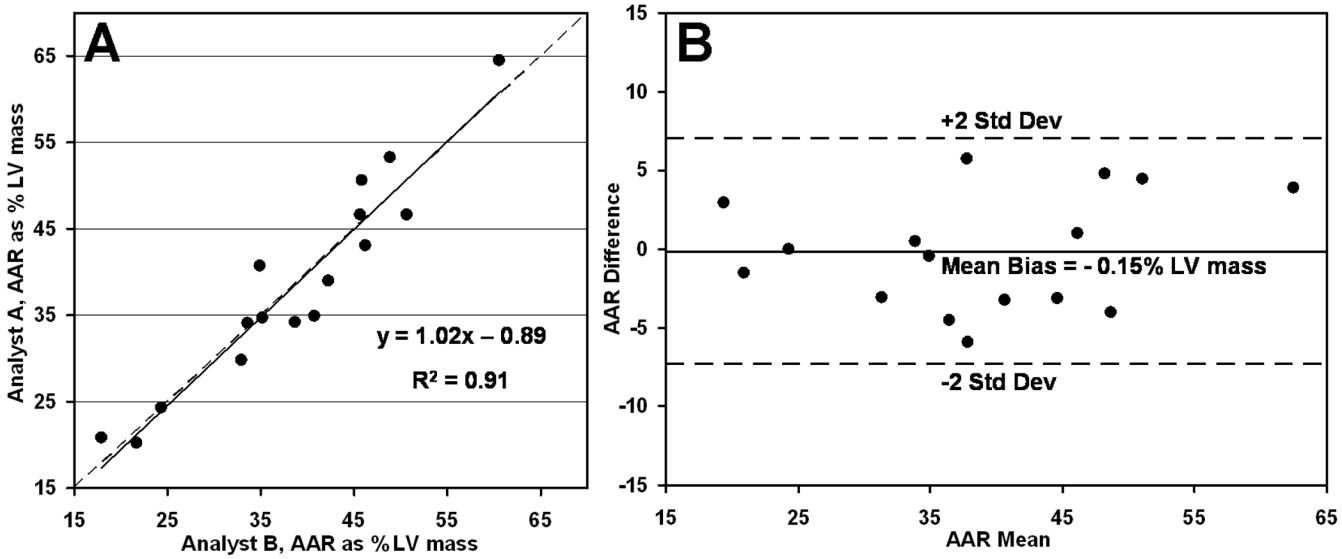

Figure 8.

Interobserver variability for T2-weighted CMR for quantifying area at risk (AAR) as percent left ventricular (LV) mass. Scatter plot of AAR measured by two different observers shows good linear agreement ($R^2 = 0.91$) over a wide range of AAR sizes (A). Corresponding Bland-Altman analysis indicates a bias of −0.15% between the two observers (B).